Hierarchical C-N doped NiO with dual-head echinop flowers for ultrasensitive monitoring of epinephrine in human blood serum

Mohammed Y. Emran[1] & Hesham Khalifa [1] & Hassanien Gomaa[1] & Mohamed A. Shenashen [1,2] & Naeem Akhtar [1] & Moataz Mekawy[1] & Ahmed Faheem[3] & Sherif A. El-Safty[1]

Abstract The authors describe nanoelectrodes based on the use of hierarchical carbon-nitrogen nanospheres and dual-head nickel oxide echinop flowers (CN@HDN) placed on indium tin oxide (ITO) electrodes. The modified electrodes enable sensitive detection of catecholamine neurotransmitters, specifically of epinephrine (EPI) in human serum samples. The modified electrodes possess many active sites along the {111} crystal plane and large contact surfaces. This enables a rapid EPI diffusion within a highly active transport surface. The geometrical and morphological structures of the NiO decorated with CN-nanospheres render superior electrocatalytic behavior at a relatively low working voltage of 0.12 V (vs. Ag/AgCl) which makes the sensor relatively specific. The use of CN also increases the electron transfer rate and facilitates mass transfer between electrolyte (EPI sample) and catalytically active sites. The electrode is sensitive, selective and works at near-physiological pH values. It has a detection limit as low as 4 nM of EPI.

Electronic supplementary material The online version of this article (https://doi.org/10.1007/s00604-017-2498-3) contains supplementary material, which is available to authorized users.

✉ Sherif A. El-Safty
sherif.elsafty@nims.go.jp

[1] Research Center for Functional Materials, National Institute for Materials Science (NIMS), 1-2-1 Sengen, Tsukuba-shi, Ibaraki-ken 305-0047, Japan

[2] Present address: Petrochemical Department, Egyptian Petroleum Research Institute (EPRI), Nasr City, Cairo 11727, Egypt

[3] School of Pharmacy and Pharmaceutical Sciences, Faculty of Health Sciences and Wellbeing, University of Sunderland, Sunderland SR1 3SD, UK

Keywords Epinephrine-sensor · Catecholamine neurotransmitters · Physiological pH · Electrochemical sensor · NiO head · Nanotubes · Jagged surface

Introduction

Epinephrine (EPI) is an abundant catecholamines [1, 2], has many biological activities, and is present in low levels in patients with Parkinson's disease and orthostatic hypotension [3–6]. High levels of EPI are associated with stress and thyroid hormone deficiency [7]. Furthermore, EPI released intensively inside the human body during perceived emergency situations. During the defensive/fighting actions, EPI supports the supply of the brain and muscles with oxygen and glucose [8]. Therefore, a selective, sensitive detection of a wide-range of EPI concentrations is crucial in neurophysiology, clinical diagnosis, and life quality.

Analytical methods for EPI include spectrophotometry, fluorimetry, liquid chromatography, capillary electrophoresis, thermal lens microscopy, chemiluminescence, electrochemiluminescence, and flow injection analysis [9, 10]. These techniques showed evidence of monitoring EPI in various samples, but they mainly associated with cumbersome procedures, expensive instrumentation, lack of selectivity, and prolonged analysis time. Among all techniques, electrochemical sensing based modified electrode is commonly employed to quantify EPI [11–13]. A controlled design of electroanalytical protocol of EPI remains challenge. To date, the materials used for electrode fabrication showed redox probes of EPI at high over potential due to the slow-moving of charges over electrode at traditional bare working electrodes (i.e., Au, Ag, Pt, glassy carbon, and graphite). Synthesis of highly reliable electrodes with fast response

binding and high molecular diffusion along the entire active coverage surfaces is demanded to sensitive and selective detection of EPI, particularly in the presence of highly comparative species such as ascorbic acid (AA) and uric acid (UA) [12–19].

Non-precious metal oxides, such as NiO, CuO, Co_yO_x, TiO_2, and Mn_yO_x, have large surface area, high porosity, hydrophilic character, and relatively good chemical and mechanical stability. They have attracted great interest because of their promising applications in catalysis, energy storage, sensor, and capacitor devices [20–28]. Among these candidates, NiO has received tremendous interest in supercapacitor and electrochemical sensor applications because of its low-cost, low toxicity, and high electrocatalytic performance [29]. However, it has high peak potentials and lake of conductivity in practical biosensing application of NiO [30]. Carbon-, nitrogen-doped metals or metal oxides offer excellent electrical conductivity and unique chemical and physical properties of nano-hybrid composites [31–34]. The carbon materials exhibit large specific surface area and good electrical conductivity. In addition, carbon materials can be functionalized with abundant carboxylic and/or hydroxyl groups and exhibit good biocompatibility. The resulting nano-hybrid composites have been used to fabricate biosensors with improved sensing performance.

In this study, hierarchical carbon-nitrogen nanospheres@dual-head nickel oxide echinop like flowers (CN@HDN) were synthesized. The HDN structure was fabricated with two dual-heads that connected throughout dipole resembling rod. The head construction is like a sea urchin with thick nanotubes spread out interiorly/exteriorly at NiO echinop head surface. The CN advanced the electrocatalytic activity of HDN related to the high impact on the surface area, pore volume and producing multi-active sites. Furthermore, The CN acts as a molecular transport between the active catalytic surface and the targeted molecules, which facilitate molecular diffusion between electrolytes and active sites at the electrode surfaces. These specific features of CN@HDN make it a superior electroactive modified electrode for catalytic oxidation of biomolecules with enhanced sensitivity and selectivity. Our protocol provides high sensitivity and selectivity for EPI-sensing. The CN@HDN can be employed for monitoring of EPI in human serum samples with high sensitivity and selectivity.

Experimental section

Materials and reagents

All chemicals are analytical grade and were used without further purification. Nickel nitrate hexahydrate ($Ni(NO_3)_2.6H_2O$), diammonium hydrogen phosphate $(NH_4)_2HPO_4$, dopamine hydrochloride (DA), uric acid (UA), epinephrine (EPI), norepinephrine (NE), potassium ferricyanide [$K_3Fe(CN)_6$], human serum, and phosphate buffer (PB; 0.1 M, pH 7.0) were purchased from Sigma–Aldrich Company, Ltd., USA (https://www.sigmaaldrich.com/japan.html/). L(+)-ascorbic acid (AA) , aniline, potassium persulphate, hydrochloric acid (HCl) were purchased from Wako Company, Ltd., Osaka, Japan (https://labchem.wako-chem.co.jp/). Indium tin oxide (ITO) glass electrodes (2 cm × 1 cm) were purchased from ALS Company, Ltd. , Japan (https://www.als-japan.com/).

Synthesis of HDN

Symmetric HDN was prepared by the one-pot hydrothermal synthetic approach. The materials were prepared as follows: 1 mM of ($Ni(NO_3)_2.6H_2O$) was dissolved in a 100 mL volumetric flask containing 15 mL of deionized water and stirred until dissolved at room temperature, followed by dropwise addition of 15 mL of 1 m M aqueous solution of $(NH_4)_2HPO_4$ to the stirred solution of ($Ni(NO_3)_2.6H_2O$) (see Scheme S1). The prepared solution was transferred into a 100 mL Teflon-lined stainless steel autoclave, sealed and maintained at 160 °C for 8 h. After the required time, a green precipitate appeared as a result of HDN and then rinsed with ultrapure water/absolute ethanol to remove the soluble impurities. The prepared material was dried in an oven at 80 °C and annealed at 400 °C for 4 h to obtain HDN.

Decorated of CN at the surface of HDN

Carbon-nitrogen nanospheres decoration of hierarchical NiO echinop flower was prepared as follow. Typically, 100 mg of the prepared HDN was dispersed under ultrasonication for 4 h in 100 mL of Tris–buffer solution (pH = 8.5) and then loaded into a 250 mL volumetric flask and stirred at room temperature. Then, purified aniline (20 mM) was added. Next, 20 mM of potassium persulfate solution was added dropwise to the stirred solution to induce polymerization reaction at 0 °C. The polymerization lasted for 12 h at room temperature, and the obtained aniline polymerized HDN were washed several times with deionized water. Finally, the polyaniline-coated HDN were calcined at 500 °C for 4 h in an argon atmosphere to obtain CN-decorated HDN.

Fabrication of working electrode

HDN and CN@HDN were fabricated as the following; i) dispersion of the prepared materials in 5 mL methanol at room temperature, ii) 15 µL solution of HDN and CN@HDN were fabricated by uniformly spreading onto the surface of an ITO glass substrate (2 cm × 1 cm). To control the exposed surface area of ITO substrate and for better electrical contact a definite

area (1 cm × 1 cm) of the ITO electrode substrate was masked prior to the deposition. This process was repeated five times; the resulting electrode was dried overnight at room temperature, followed by washing with deionized water to remove any unbound particles.

Human serum analysis using CN@HDN-modified electrode

The real application was performed using standard addition method in human serum samples. Human serum was purchased from Sigma Aldrich and strode at refrigerator at −20 °C until used. The human serum samples were diluted 20 times using 0.1 M PBS (pH 7.0). 500 μl of the serum sample was added to 9.5 mL of PB to perform chronoamperometric at applied potential 0.12 V with successive addition of EPI concentrations under N_2 saturated at room temperature.

Results and discussion

With aiming to synthesis low-cost, yet effective, modified electrode, NiO is an ideal candidate compared with Au nanoclusters, Au nanoparticles, ZnO-gC_3N_4, and MoS_2 (see Table S1) [31–34]. In our protocol, the CN-modified HDN enhances the electron clouds and active charges along {111} NiO crystal plane, leading to strong interaction between the negatively-charged (CN@HDN) surface and the positively-charged molecules (EPI) at optimal sensing conditions. The design of CN@HDN-modified electrode makes (i) the mass transfer between the electrolyte (EPI sample) and bare electrode interface, (ii) and the binding of EPI at the electrode surface more facile. Building electrode based hierarchical CN/NiO with dominant mesoporous structures, and dual-head echinop flowers associated with abundant nanotubes creates electrode surfaces with highly interactive binding with molecular target during the electrocatalytic oxidation of EPI.

Formation of HDN and CN@HDN

The newly designed morphological growth of hierarchical NiO combines with the desired nanostructures using structure-directing agent templates $(NH_4)_2HPO_4$) under hydrothermal treatment conditions was prepared (see Scheme S1). The initial precursors were ($Ni(NO_3)_2.6H_2O$, $(NH_4)_2HPO_4$), and the HDN can be produced by successive reactions. In a typical procedure, hydrolysis of $(NH_4)_2HPO_4$ creates OH^-, and PO_4^{3-} anions which subsequently reacted with Ni^{2+} to form hierarchical NiOOH with controlled structure. These anions subsequently reacted with Ni^{2+} ions to form (i) active construction of NiOOH, (ii) nickel oxide echinop flower like with two heads assembled horizontally in opposite direction, and (iii) formation of thick nanotubes- resembled structure. PO_4^{3-} anions are a highly dense negative charge, which acts as a mediator for crystal growth. The electrostatic attraction between positive-charged Ni^{2+} ions and negative-charged PO_4^{3-} ions was a pushy force to generate hierarchical echinop flower shaped structures with dual heads and trunk (see Fig. 1 & Scheme S1). Controlling head construction may attribute to the stereo PO_4^{3-} shape in its solution, which reflected the crystal growth depth from the inner to outer surface. The CN was assembled after the stable construction of HDN, in which a thin film of polyaniline polymerized at 0 °C after dropwise addition of potassium persulfate with continuous stirring. Potassium persulfate initiates the free radical monomer, continuous stirring forms black precipitates from poly aniline decorated hierarchical NiO. Carbonization of polyaniline acts as the CN source at 500 °C in Ar gas flow leads to homogenous CN decorated HDN.

In general, the morphological and chemical compositions of CN@HDN are directly responsible for efficient electro-oxidation of EPI in human serum blood as presented in Scheme 1. The prepared material hierarchy along the {111} crystal facets might lead to suitable accommodation of sensitive and selective EPI detection as a result of high surface area, large surface contact with the target's electrolyte, and easy molecular transport at the electrode–electrolyte interface.

Characteristic features of the designed HDN and CN@HDN

Field emission- scanning electron microscope (FE-SEM) and high resolution-transmission electron microscope (HR-TEM) were used to investigate the geometrical and morphological structure of the synthesized materials. Figure 1a and its inset show the FE-SEM of NiO, which revealed that the overall geometrical structure is like echinop flower shape with two similar heads connected by a rod with uniform and homogeneous shape. The head shape is like a half-circle with a jagged surface like tubular ends of echinop flower. HDN has two similar heads with an average size of 3–4 μm connected by a rod with an average size of 1.5–2 μm, as illustrated in Fig. 1b, c, and provides the CN nanospheres decorate the HDN surface. FE-SEM mapping illustrates surface atomic composition, where Ni, O, C, and N homogeneously and uniformly dispersed on the surface of the NiO, as shown in (Fig. 1(Da, Db, Dc, and Dd)). High magnification of HR-TEM illustrates that the head morphology is roughly similar to a rough sea urchin surface and like a tubular echinop flower. As shown in Fig. 1e–g, the head surface contains a thick nanotube spreading from the deep to the outer surface. The CN cover the entire surface without influencing the head morphology but the influence on the surface area and pore volume. High magnification of high angle annular dark field-scanning transmission electron microscopy (HAADF-STEM) at one spot focusing

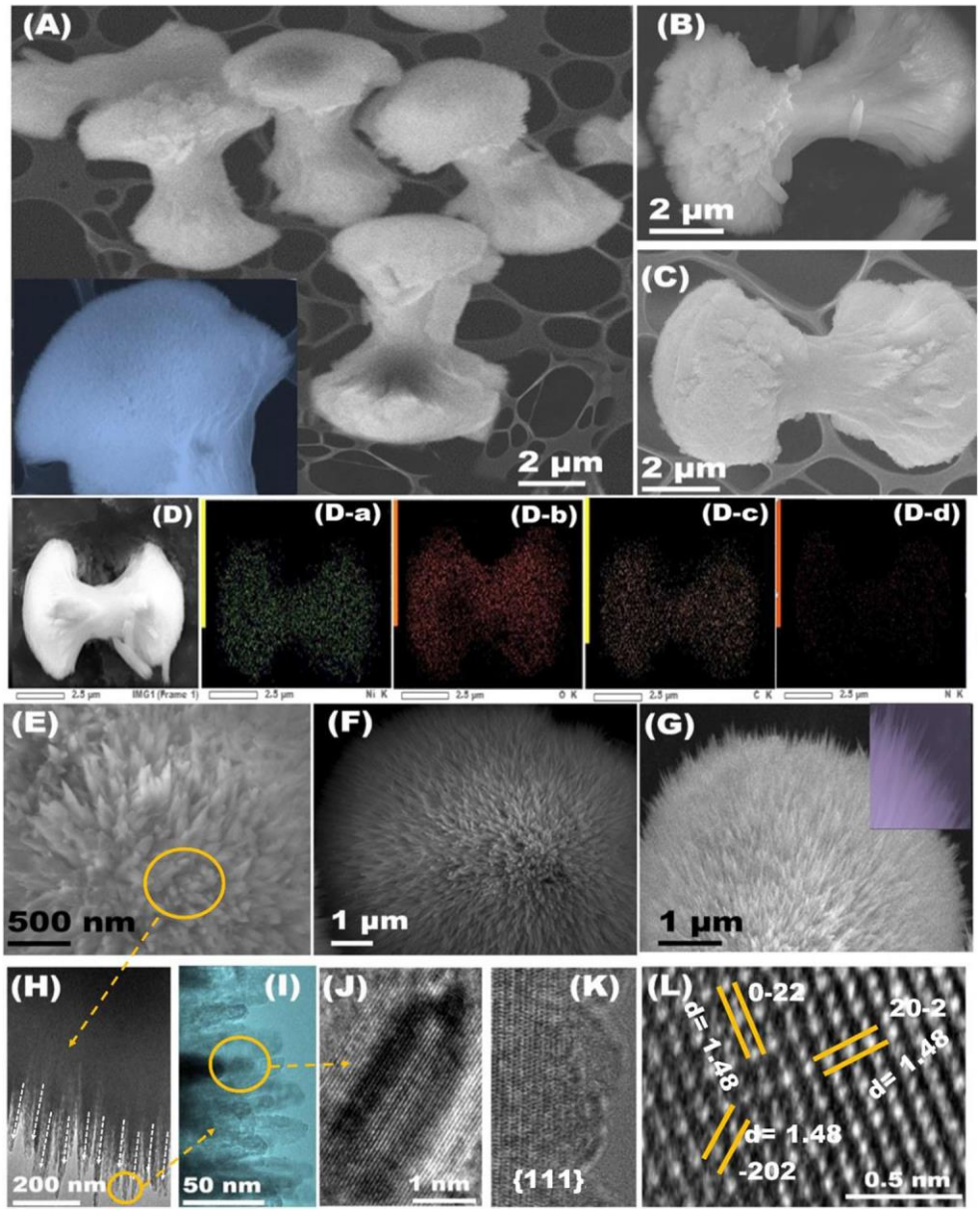

Fig. 1 a FE-SEM of CN@HDN and (b & c) high magnification of FE-SEM for the different unit in different position for obtaining the geometry and unity. (Da-Dd) the FE-SEM mapping for Ni, oxygen, carbon, and nitrogen, respectively. (e–g) HAADF-STEM focusing on the head surface geometry and morphology. (h & i) High magnification of HAADF-STEM focusing on the dead ends which like a tube covered by nitrogen doped carbon. j Highly magnification of HAADF-STEM focused on the nanotube surface illustrated that the mesoporous surface structure. (k & l) reflect ED-STEM at the CN@HDN to obtain the degree of crystalline structure at the outer head surface around {111} crystal plane

on the nanotube at the head surface illustrates its specific features, where the tube size ranged from 15 to 20 nm and decorated with a thin layer of CN (Fig. 1h, i). High magnification of HAADF-STEM-focused on the head nanotubes obtains porosity with average pore size 5.5 nm, which consequently revealed the unique morphology (Fig. 1j–l), and outline the HDN surface is controlled with high crystalline surface structure.

Atomic configurations and surface electrons in continuous generation modes around the active sites for the {111} crystal plane for HDN and CN@HDN using density functional theory (DFT) are illustrated in Fig. 2. Figure 2a shows that mesostructured pore windows formed around {111}-crystal facets were taken perpendicular to the fourfold axis. The tilt modeling pronounced the atomic-scale arrangement at the center and edge of the crystal lattice of the entire tube-shaped layer. The mesoporous structure provides open pores which directly affected the electrocatalytic nature by influencing charge transfer and mass transport, leading to rapid and strong binding with the target biomolecules. Continuous double layers of electron streams on the top-level isosurface of the {111} orientation of HDN are distributed close to a central and focal point surface around Ni^{2+} and O^{2-} vacancy sites (Fig. 3b). Figure 2c shows the CN cloud charge surface around the {111}-crystal plane around the single-layer Ni and O atom organization on the top surface. The CN changes the characteristic charges of the surface around Ni^{2+} and O^{2-} vacancy sites leading to low energetic contact for the HDN surface and increases dominant electron-rich O^{2-} vacancy sites for top 4 Ni^{2+} and O^{2-}. The electrostatic potential

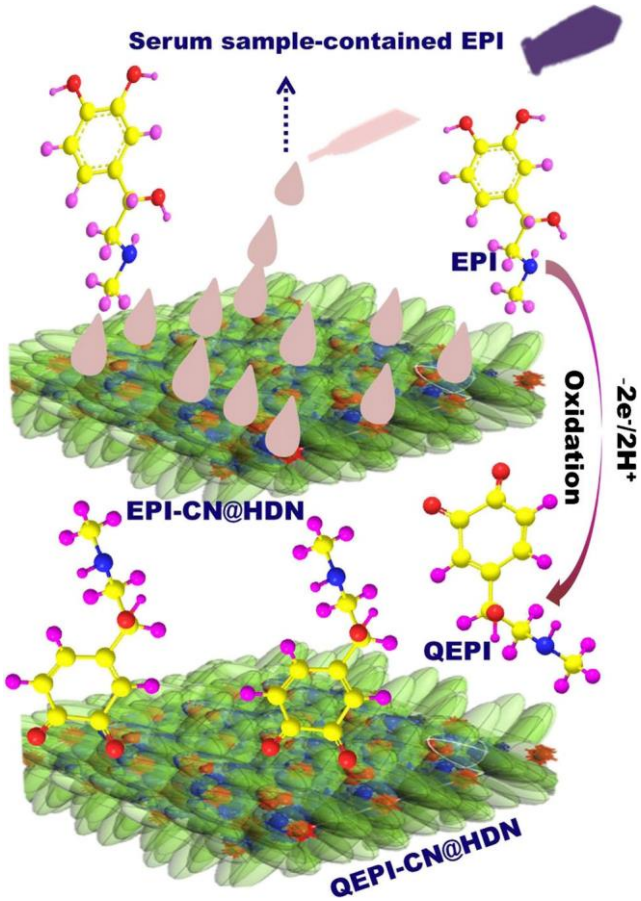

Scheme 1 The electrochemical oxidation mechanism of epinephrine in human serum at the top surface of CN@HDN with corresponding {111} crystal plane, where EPI form changed to EPI quinone form

(ESP) mapping of the {111}-exposed plane surfaces strongly suggest that the top surface of Ni^{2+} and O^{2-} atoms near the vacancy sites are charge-rich isosurfaces (Fig. 2d, e) for HDN and CN@HDN, respectively. The possible local bonding environments and orientations of ESP around one- and two-Ni^{2+}-center sites that aligned perpendicular to the top-surface matrix are demonstrated by DFT (Fig. 2c, e). The surface represents localized networks of ESP confinement and elevated the surface charge density around C, N, O, and Ni atoms and effective potential EPI-to-Ni^{2+} site binding (Fig. 3d, f). This geometric molecule-to-surface orientation generated numerous accessible surface active sites, flexible interactions, and thermodynamically stable bindings. The surface configurations of hierarchically oriented HDN with nanotubes and open holes and longitudinal long-range channels can feasibly create dense Ni^{2+} atoms and more electron-rich O^{2-} vacancy sites, producing more efficient electron transport; hence, The CN facilitates the mass transport and effective binding of target molecules at the {111}-exposed plane.

Crystal formation of hierarchical HDN and CN@HDN were investigated via wide angel-XRD analysis within the range 20°–80°. Figure S1A shows the WA-XRD spectra which reflect a series of diffraction peaks centered at 2θ = 37.17°, 43.2°, 62.73° and 75.4°corresponding to (111), (200), (311), and (222) crystal planes of face-centered cubic NiO (JCPDS no. 01–089-5881), respectively [26, 27, 29]. The carbon peak is presented at 2θ = 29.68°, and it can be assigned to the (200) diffraction [24]. The peak intensity diffraction of CN@HDN is lower than that of HDN, which further confirms the presence of CN on the surface of HDN with unity and formality.

Confirmations of CN-nanospheres are illustrated from the Raman spectra of the HDN and CN@HDN samples. The Raman spectra for HDN and CN@HDN were performed at an excitation wavelength of 532 nm, time exposure of 3 s, and repeated for 10 times. Figure S1B shows the vibrational band at approximately 539, 773, and 1076 cm^{-1} caused by (1P) (TO), (2P) (2TO), and (2P) (2LO) phonons and modes, respectively, indicating the presence of NiO [31]. However, the existence of two distinct peaks in CN@HDN corresponding to D (~1366 cm^{-1}) and G (~1500 cm^{-1}) bands originated from the disordered carbon and sp2 cluster, respectively [35]. The porous nature and surface area measurements of HDN and CN@HDN were investigated by N_2 adsorption-desorption isotherm. Figures S1C and S1D show the N_2adsorption-desorption isotherm and the NLDFT distribution graph, which reveal that the HDN and CN@HDN have hierarchical structures as a result of the presence of meso- and macropores distributed throw HDN surface (for more details see electronic supplementary materials). Furthermore, the elucidations of HDN and CN@HDN surface components were performed by XPS measurements, where high-resolution XPS spectra of the Ni 2p, O 1 s, C 1 s, and N 1 s peaks provide the chemical formations of CN@HDN (for more details see Fig. S2 and the electronic supplementary materials).

Electrocatalytic activity of the designed electrodes

The overall electrocatalytic activity of the designed electrode was demonstrated using cyclic voltammetry in phosphate buffer (pH 7.0) containing 1 mM $[Fe(CN)_6]^{3-}$ within the potential range of 0.0 to 0.7 V (vs. Ag/AgCl) at scan rate of 100 mVs^{-1} (Fig. 3a). $[Fe(CN)_6]^{3-}$ was used as a redox probe to investigate several factors, including electronic properties and surface chemistry which directly change the kinetic properties [35]. As shown in Fig. 3a, a negative shift in redox peaks for CN@HDN-modified electrode and high redox response current is obtained with low redox peak separation potentials (ΔEp) for the CN@HDN-modified electrode (100 mV) compared with HDN (151 mV). Thus, the CN@HDN-modified electrode can be attributed to enhance ion transmission performance at the electrode–electrolyte interface, thereby engaging greater fractions of catalytic active sites on the surface of the electrode for the Faradaic redox reaction.

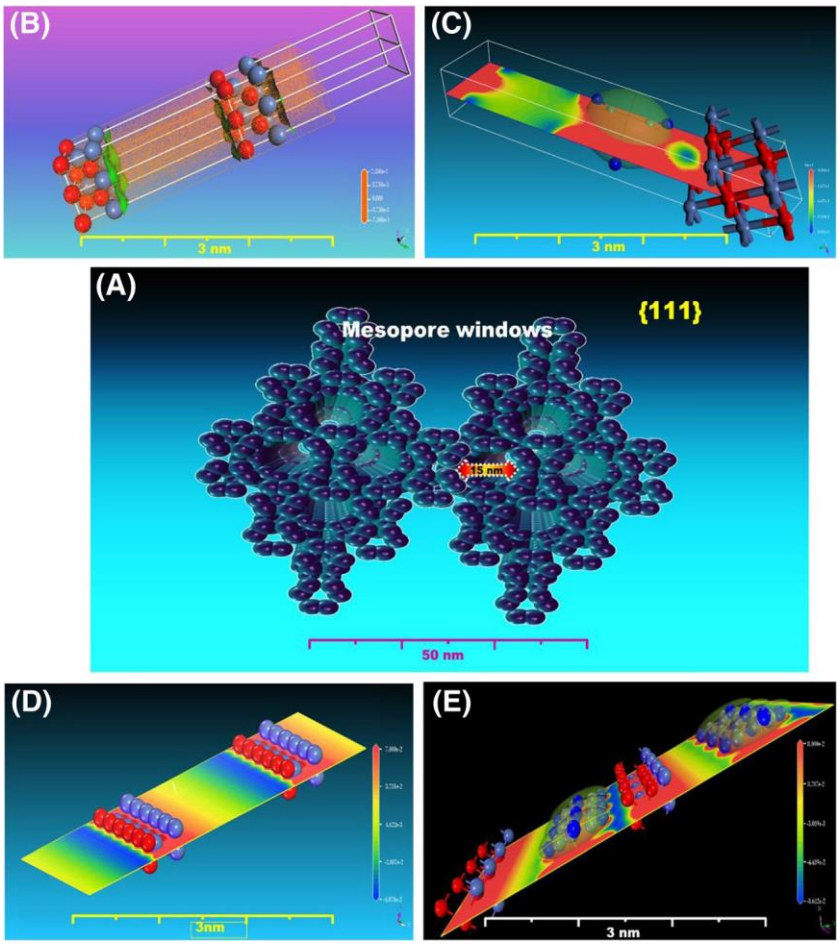

Fig. 2 a Mesostructured {111}-HDN crystal facet oriented around the mesoporous frameworks. The location of the frame structure along {111} plane enabled the actively energetic surface coverage for facile diffusion and strong binding with the target molecules. b Ball and stick model for top-view of single layer CN-HDN atomic organization along with {111} crystal plane. The double and single layer of the atomic organization of HDN crystal into exposed {111} surface plane with Ni and O represent the contact and possibly of the binding with target molecules with and without CN. c High energy surfaces formed along the entire HDN crystal structure directed along {111} surface exposure for HDN. d The long-domain surface configuration with cloudily electronic surface density enabled the facile diffusion of electrons, and charges without constraints along the crystal structures and {111} plane for CN@HDN. e The orientation of building atomic tower shows the possibility of the {111}-top-surface binding sites with high densely electronic clouds with the crystal edge surface and central crystal corresponding to density functional theory (DFT) with the effectiveness of CN on the surface atomic construction and contact with the biomolecules

The interfacial electron-transfer rate was measured using impedance microscopy (EIS) to decouple the enhanced electrocatalytic activity of the HDN-modified electrode and the effect of CN at its surface. In an EIS measurement, the semicircle diameter reflects the electron transfer resistance (Ret) of the electrode, and the line reflects the diffusion of the electroactive species. In general, a large semicircle means a high charge transfer resistance of the electrode, implying a low electron transfer rate (higher resistivity). Typical Nyquist impedance plots of HDN and CN@HDN-modified

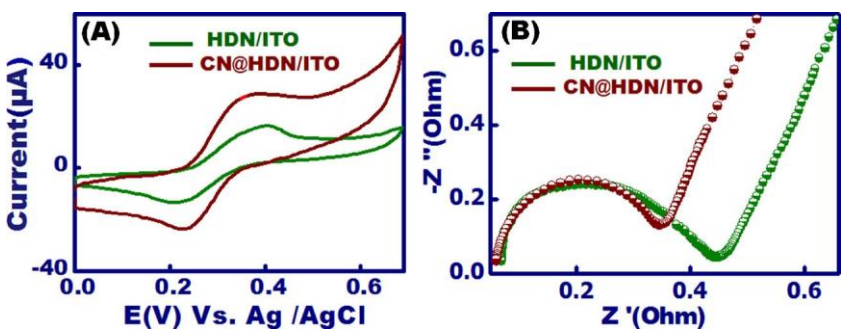

Fig. 3 a CV of of HDN (olive line) and CN@HDN (wine line)-modified electrodes in phosphate buffer containing 1 mM of $[Fe(CN)_6]^{3-}$ at 100 mVs^{-1}. b Nyquist electrochemical impedance plots of (olive scatter) HDN and (wine scatter) CN@HDN-modified electrodes in phosphate buffer.

electrodes in a buffer solution (pH 7.0). The CN@HDN-modified electrode (Fig. 3b blue line) precedes a small semicircle diameter at high frequency, showing a relative small Ret compared with HDN, which may be related to the presence of NC decorated HDN as a result of its electron-transport efficiency.

Electrochemical statements of the designed electrodes for EPI, AA, NE, DA, and UA

The monitoring and evaluation of the electrocatalytic activity of HDN and CN@HDN-modified electrode for electrooxidation of EPI, AA, NE, DA, and UA were performed using differential pulse voltammetry (DPV) in phosphate buffer at a scan rate of 100 mVs^{-1}, pulse height of 60 mV, step height of 5 mV, pulse distance of 200 ms, and pulse width of 25 ms. As illustrated in Fig. S3A, the catalytic oxidation of EPI on HDN and CN@HDN-modified electrode was performed, and a significant enhancement of the current value appeared at 0.12 V for CN@HDN-modified electrode. The same behavior was observed with AA, NE, DA, and UA where the catalytic oxidation current of CN@HDN was higher than that of HDN at potential values of 0.05, 0.17, 0.4, and 0.47 V in phosphate buffer for AA, NE, DA, and UA respectively, as in Fig. S3 (B–F). The peak current intensity values are 91.96, 82.15, and 80.31 μA for 10 μM DA, 10 μM NE, and 10 μM DA, respectively at the CN@HDN–modified electrode, while these intensity values are 10 and 16.3 μA for AA and UA, respectively. The high response of CN@HDN-modified electrode for EPI, NE, and DA than AA and UA reveal that the fabricated electrode has high sensitivity for catecholamine neurotransmitters and every molecule has specifically applied potential. The sensitivity and selectivity of the CN@HDN-modified electrode may be related to its high surface area pore distribution, unique structure with numerous active sites, and easy molecular adsorption/diffusion at the electrode surface.

Electrochemical detection of EPI, AA, NE, DA, and UA

To evaluate and demonstrate the sensitivity and selectivity of the CN@HDN-modified electrode for epinephrine, we calculate the detection limit of EPI and other co-existing molecules by adding various concentrations of each molecule using DPV in phosphate buffer (pH 7) at a scan rate of 100 mVs^{-1}, pulse height of 60 mV, step height of 5 mV, pulse distance of 200 ms, and pulse width of 25 ms. Figure 4a shows the monitoring of CN@HDN-modified electrode sensitivity toward EPI, where the peak current increased as EPI concentrations increased in the linear range (1–32 μM). By plotting concentration versus the current, a linear relationship was observed as in the inset in Fig. 4a with regression equation of I(μA) = 55.6 + 35.12 [EPI] (μM) (correlation coefficient R^2 = 0.87) (S/N = 3). The detection limit was calculated to be 0.37 μM. The same behavior for AA, NE, DA, and UA were observed. The peak current response was increased as each molecule concentration is increased ranging from 0.05–2 mM, 5–50, 1–32, and 25–600 μM for AA, NE, DA, and UA, respectively, as shown in Fig. 4b–e. A linear relationship is observed by plotting the concentrations of AA, NE, DA, and UA (μM) vs the currents (μA). The regression equations are presented as follow: I (μA) = 0.021 [AA] (μM) + 19.7; R^2 = 0.99}, I(μA) = 31.93 + 0.41 [NE] (μM) (R^2 = 0.89), I(μA) = 33.48 + 0.59 [DA] (μM)(R^2 = 0.87), and {I (μA) = 26.62 + 0.73 [UA] (μM); R^2 = 0.99}, where the detection limit was 36, 3, 1.8, and 15 μM for AA, NE, DA, and UA, respectively. These studies confirm the sensitivity of CN@HDN-modified electrode for monitoring of EPI compared to the co-existing molecules. Further confirmation of selectivity obtained from Fig. 4f at 1, 5, 10, and 20 μM of EPI indicates that no concentration was detected for AA and UA, while other molecules such as NE and DA have less sensitivity than EPI. Thus, CN@HDN-modified electrode exhibit high sensitivity and selectivity for monitoring of EPI.

Amperometric signaling of EPI on CN@HDN-modified electrode

The chronoamperometric technique was used at an applied potential of 0.12 V in PB to evaluate the electrocatalytic activity of C N@HDN-modified electrode for quantification of EPI under dynamic conditions. The CN@HDN-modified electrode exhibits excellent and fast amperometric response through the addition of EPI with a dynamic linear range from 1 to 5 μM (Fig. 5a). From the calibration curve of the plot of the concentration addition versus the responded current, a linear relationship was obtained with regression equation, namely, I(μA) = 1.65 + 11.38 [EPI] (μM), R^2 = 0.999. The relative standard deviation (RSD) was estimated to be 1.5% with low detection limit up to 4 nM. Thus, CN@HDN-modified electrode high sensitivity for EPI detection and can be potentially used to determine EPI in human serum samples.

Application of CN@HDN-modified electrode for EPI monitoring in human serum sample

Epinephrine detection in human serum samples was investigated to ensure analytical and clinical application of the assembled electrode. Standard addition method was used, where 50 μL of the serum sample was added to 10 mL of PB by stepwise addition of EPI concentrations (1–5 μM) to the sample solution using the amperometric method at an applied potential of 0.12 V on the CN@HDN-modified electrode. Sensitive relative peaks with step addition of EPI obtain a high sensitivity of for EPI in analytical real samples (Fig. S4). Further confirmation of the possibility of clinical application of the using CN@HDN-modified electrode is clearly

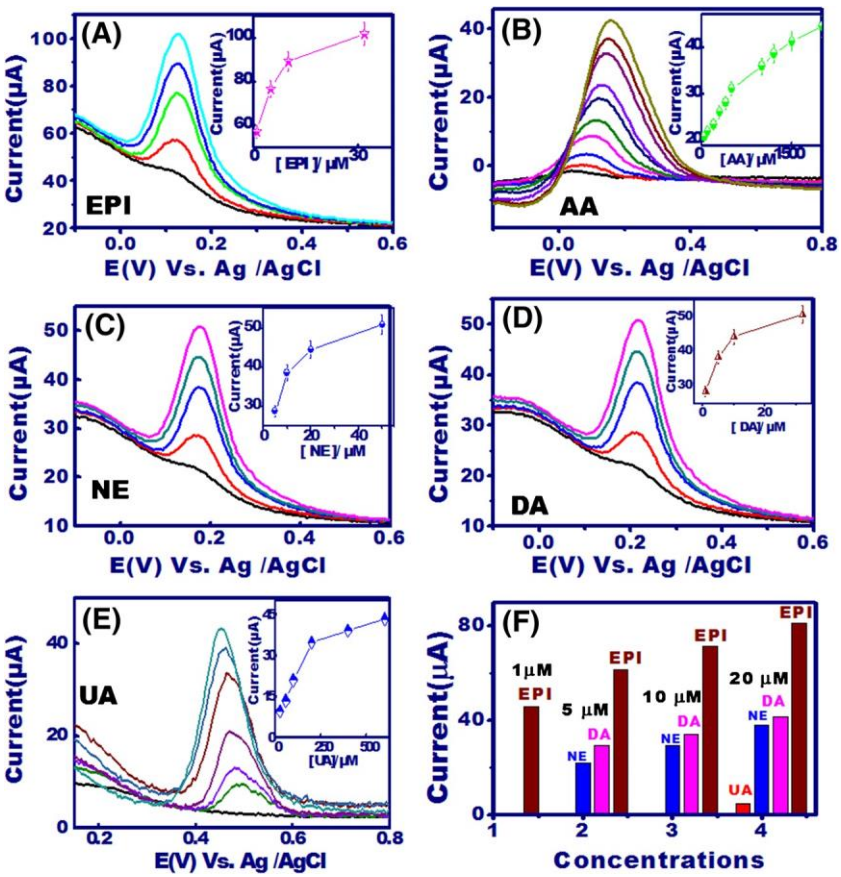

Fig. 4 DPV curves of (a) EPI concentrations (1–32 μM), its inset the plot of [EPI](μM) vs the current (μA). b AA concentrations (0.05–2 mM), and its inset the plot of AA concentration (μM) vs the current (μA). c NE concentrations of (1–50 μM), and its inset the plot of [NE](μM) versus the current (μA). d DA increasing concentrations (1–32 μM), and its inset the plot of [DA](μM) vs the current (μA). e UA concentrations (25–600 μM), and its inset the plot of [UA](μM) vs the current (μA) of CN@HDN-modified electrode in phosphate buffer (pH 7) at scan rate 100 mVs^{-1}, pulse height 60 mV and pulse width 25 ms. f The column plots of different concentrations of all analytes (1, 5, 10 and 20 μM) vs the current (μA) for obtaining the electrode selectivity of EPI at low concentrations

shown in Table 1, where the recovery percentage for human serum sample ranged from 92 to 97% with %RSD of 2.7. These results clearly confirmed that CN@HDN-modified electrode is a candidate promising modified electrode for EPI monitoring in real samples and can be employed for clinical application.

Stability and reproducibility

The reproducibility of the CN@HDN-modified electrode was evaluated. In such experimental protocols, current responses are examined for various (≥10) CN@HDN-modified electrode at 10 μM EPI concentration under optimum sensing conditions in phosphate buffer and 0.12 V (vs. Ag/AgCl) of applied potential at room temperature. The RSD of the 10th amperometric response assays range 1.7%–2.25%, as evidenced by the fitting plot of the response current graphs (Fig. S5A). Current responses of the 10th different samples with a constant concentration of EPI (10 μM) were measured repeatedly after every washing of CN@HDN-modified electrode with distilled H_2O, which was conducted three times under optimum sensing conditions, to confirm the reusability of the CN@HDN-modified electrode (Fig. S5B). As a result, the reused CN@HDN-modified electrode showed high-sensing response efficiency (i.e., 98%) despite ten reuses/cycles. The designed electrode is highly stable even after 10 uses, and its reusability raises economic valuation.

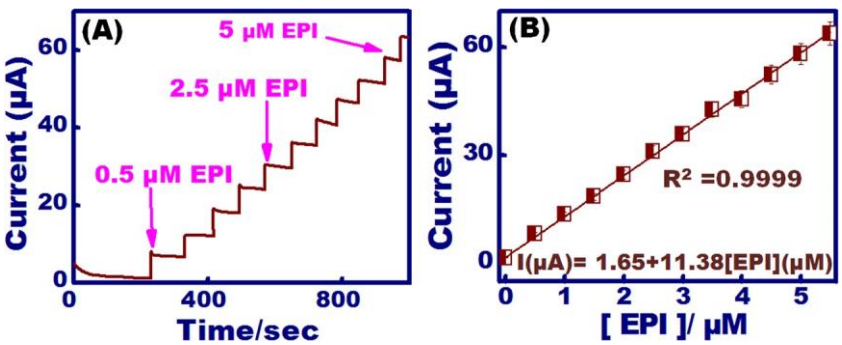

Fig. 5 a Amperometric response of the CN@HDN-modified electrode to successive addition of 0.5 μM epinephrine over the concentration range from 1 to 5 μM at 0.12 V, and (b) the corresponding calibration plot

Table 1 Determination of EPI in human serum samples collected from a volunteer

Sample	EPI[a] added μM/L^{-1}	EPI[b] found μM/L^{-1}	%R[c]
Serum sample	1	0.95 ± 0.001	95
	2	1.8 ± 0.003	90
	3	2.83 ± 0.005	94
	4	3.88 ± 0.001	97
	5	4.6 ± 0.002	92

The quantitative analyses of EPI were carried out by spiking it with concentration in the range of 1–5 μmol L^{-1} on CN@HDN-modified electrode. The standardization analyses of targets were determined according to amperometric techniques at 0.12 V, and repeated 3 times per each sample analysis

[a] Epinephrine added to the prepared samples (C_A)

[b] Epinephrine found at the presented calibration curve (C_F)

[c] %Recovery is the percentage of recovery ($\%R = C_F / C_A \times 100$)

Conclusions

The sensitive and the selective electrode were successfully fabricated for monitoring of EPI in human blood serum using a novel hierarchical carbon-nitrogen nanospheres decorated hierarchical NiO echinop flower like with dual heads. The CN@HDN provides high electrocatalytic activity may relate to the large surface area, easy diffusion of molecules through pores and interfacial contact of dominant Ni^{2+} on the modified electrode surface. HDN illustrates a novel morphological-shaped echinop flower with symmetric dual-heads that connected horizontally in opposite direction throughout a stick resembling rod in-between. Furthermore, the HDN heads resembled rough sea urchin surface and composed of dense nanotubes that aligned vertically along the whole head surface. The doping of CN into HDN did not alter or damage the hierarchical structures, enhanced the surface features and parameters, and enabled high adsorption/diffusion of bioactive molecules. The designed CN@HDN-modified electrode exhibits high sensitivity up to 4 nM and selective monitoring of EPI in human blood serum. The significant stability and reproducibility of our electrode design indicate that CN@HDN modified electrode can be employed for monitoring of EPI in real human blood serum and clinical diagnosis.

Compliance with ethical standards The author(s) declare that they have no competing interests.

References

1. Robinson DL, Venton BJ, Heien MLAV, Wightman RM (2003) Detecting subsecond dopamine release with fast-scan cyclic voltammetry in vivo. Clin Chem 49:1763–1773. https://doi.org/10.1373/49.10.1763
2. Hefco V, Yamada K, Hefco A, Hritcu L, Tiron A, Nabeshima T (2003) Role of the mesotelencephalic dopamine system in learning and memory processes in the rat. Eur J Pharmacol 475:55–60. https://doi.org/10.1016/S0014-2999(03)02115-0
3. Jemelkova Z, Barek J, Zima J (2010) Determination of epinephrine at different types of carbon paste electrodes. Anal Lett 43:1367–1376. https://doi.org/10.1080/00032710903518773
4. Shahrokhian S, Khafaji M (2010) Application of pyrolytic graphite modified with nano-diamond/graphite film for simultaneous voltammetric determination of epinephrine and uric acid in the presence of ascorbic acid. Electrochim Acta 55:9090–9096. https://doi.org/10.1016/j.electacta.2010.08.043
5. Niu LM, Luo HQ, Li NB (2005) Electrochemical behavior of epinephrine at a Penicillamine self-assembled gold electrode, and its analytical application. Microchim Acta 150:87–93. https://doi.org/10.1007/s00604-005-0331-x
6. Lu X, Li Y, Du J, Zhou X, Xue Z, Liu X, Wang Z (2011) A novel nanocomposites sensor for epinephrine detection in the presence of uric acids and ascorbic acids. Electrochim Acta 56:7261–7266. https://doi.org/10.1016/j.electacta.2011.06.056
7. Ghica ME, Brett CMA (2013) Simple and efficient epinephrine sensor based on carbon nanotube modified carbon film electrodes. Anal Lett 46:1379–1393. https://doi.org/10.1080/00032719.2012.762584
8. Beitollahi H, Karimi-Maleh H, Khabazzadeh H (2008) Nanomolar and selective determination of epinephrine in the presence of norepinephrine using carbon paste electrode modified with carbon nanotubes and novel 2-(4-oxo-3-phenyl-3, 4-dihydroquinazolinyl)-N′-phenyl-hydrazinecarbothioamide. Anal Chem 80(9848–98):51. https://doi.org/10.1021/ac801854j
9. Goyal RN, Bishnoi S (2011) A novel multi-walled carbon nanotube modified sensor for the selective determination of epinephrine in smokers. Electrochim Acta 56:2717–2724. https://doi.org/10.1016/j.electacta.2010.12.047
10. Babaei A, Sohrabi M, Afrasiabi M (2012) A sensitive simultaneous determination of epinephrine and Piroxicam using a glassy carbon electrode modified with a nickel hydroxide nanoparticles/multiwalled carbon nanotubes composite. Electroanalysis 2:2387–2394. https://doi.org/10.1002/elan.201200483
11. Justino DDA, Lage LA, Souto DEP, Silva JV, Santos WTP, Luz RCS, Damos FS (2013) Study of the effects of surface pKa and electron transfer kinetics of electroactive 4-nitrothiophenol/4-mercaptobenzoic acid binary SAM on the simultaneous determination of epinephrine and uric acid. J Electroanal Chem 703:158–165. https://doi.org/10.1016/j.jelechem.2013.05.024
12. Sanghavi BJ, Mobin SM, Mathur P, Lahiri GK, Srivastava AK (2013) Biomimetic sensor for certain catecholamines employing copper(II) complex and silver nanoparticle modified glassy carbon paste electrode. Biosens Bioelectron 39:124–132. https://doi.org/10.1016/j.bios.2012.07.008
13. Shahrokhian S, Ghalkhani M, Amini MK (2009) Application of carbon-paste electrode modified with iron phthalocyanine for voltammetric determination of epinephrine in the presence of ascorbic acid and uric acid. Sensors Actuators B Chem 137:669–675. https://doi.org/10.1016/j.snb.2009.01.022
14. Zhang HM, Zhou XL, Hui RT, Li NQ, Liu DP (2002) Studies of the electrochemical behavior of epinephrine at a homocysteine self-assembled electrode. Talanta 56:1081–1088. https://doi.org/10.1016/S0039-9140(01)00642-7
15. Fouad DM, El-Said WA (2016) Selective electrochemical detection of epinephrine using gold nanoporous film. J Nanomater 2016. https://doi.org/10.1155/2016/6194230
16. Kim SH, Lee JW, Yeo IH (2000) Spectroelectrochemical and electrochemical behavior of epinephrine at a gold electrode. Electrochim Acta 45:2889–2895. https://doi.org/10.1016/S0013-4686(00)00364-9

17. Zhang H, Wang X, Wan L, Liu Y, Bai C (2004) Electrochemical behavior of multi-wall carbon nanotubes and electrocatalysis of toluene-filled nanotube film on gold electrode. Electrochim Acta 49:715–719. https://doi.org/10.1016/j.electacta.2003.09.023
18. Valentini F, Palleschi G, Lopez Morales E, Orlanducci S, Tamburri E, Terranova ML (2007) Functionalized single-walled carbon nanotubes modified microsensors for the selective response of epinephrine in presence of ascorbic acid. Electroanalysis 19:859–865. https://doi.org/10.1002/elan.200603788
19. Agboola BO, Ozoemena KI (2008) Efficient Electrocatalytic detection of epinephrine at gold electrodes modified with self-assembled Metallo-Octacarboxyphthalocyanine complexes. Electroanalysis 20:1696–1707. https://doi.org/10.1002/elan.200804240
20. Hoa ND, El-Safty SA (2001) Synthesis of mesoporous NiO Nanosheets for the detection of toxic NO_2 gas. Chem A Eur J 17: 12896–12901. https://doi.org/10.1002/chem.201101122
21. Shenashen MA, El-Safty SA, Elshehy EA (2011) Architecture of optical sensor for recognition of multiple toxic metal ions from water. J Hazard Mater 260:833–843. https://doi.org/10.1016/j.jhazmat.2013.06.025
22. EL-Safty SA, Abdelllatef A, Ismeal M, Shahat A (2013) Optical Nanosphere sensor based on Shell-by-Shell fabrication for removal of toxic metals from human blood. Adv Healthc Mater 2:854–862. https://doi.org/10.1002/adhm.201200326
23. Das SK, El-Safty SA (2013) Development of mesoscopically assembled sulfated zirconia nanoparticles as promising heteroge- neous and recyclable biodiesel catalysts. Chem Cat Chem 5: 3050–3059. https://doi.org/10.1002/cctc.201300192
24. Hassen D, Shenashen MA, El-Safty SA, Selim MM, Isago H, Elmarakbi A, El-Safty A, Yamaguchi H (2016) Nitrogen-doped carbon-embedded TiO_2 nanofibers as promising oxygen reduction reaction electrocatalysts. J Power Sources 330:292–303. https://doi.org/10.1016/j.jpowsour.2016.08.140
25. Yu S, Peng X, Cao G, Zhou M, Qiao L, Yao J, He H (2012) Ni nanoparticles decorated titania nanotube arrays as efficient nonenzymatic glucose sensor. Electrochim Acta 76:512–517. https://doi.org/10.1016/j.electacta.2012.05.079
26. Khairy M, El-Safty SA, Ismael M, Kawarada H (2012) Multidirectional porous NiO nanoplatelet-like mosaics as catalysts for green chemical transformations. Appl Catal B Environ 123-124:162–173. https://doi.org/10.1016/j.apcatb.2012.04.021
27. Khairy M, El-Safty SA (2013) Mesoporous NiO Nanosheets for the catalytic conversion of organic contaminants. Current Catalysis 2: 17–26. https://doi.org/10.2174/2211544711302010005
28. Khairy M, El-Safty SA, Shenashen MA, Elshehy EA, Warkocki W, Sakai M (2015) Optical mesoscopic membrane sensor layouts for water-free and blood-free toxicants. Nano Res 8(10):3150–3163. https://doi.org/10.1007/s12274-015-0815-x
29. Khairy M, El-Safty SA (2013) Mesoporous NiO nanoarchitectures for electrochemical energy storage: influence of size, porosity, and morphology. RSC Adv 3:23801–23809. https://doi.org/10.1039/C3RA44465A
30. Khairy M, El-Safty SA (2015) Promising supercapacitor electrodes based immobilization of proteins onto macroporous Ni foam materials. Journal of Energy Chemistry 24:31–38. https://doi.org/10.1016/S2095-4956(15)60281-9
31. Zhao S, Zhang J, Li Z, Zhang P, Li Y, Liu G, Wang Y, Yue Z (2017) Photoelectrochemical determination of hydrogen peroxide using a gold electrode modified with fluorescent gold nanoclusters and graphene oxide. Microchim Acta 184:677–686. https://doi.org/10. 1007/s00604-016-2035-9
32. Xi X, Li J, Wang H, Zhao Q, Li H (2015) Non-enzymatic photoelectrochemical sensing of hydrogen peroxide using hierarchically structured zinc oxide hybridized with graphite-like carbon nitride. Microchim Acta 182:1273–1279. https://doi.org/10.1007/s00604-015-1448-10
33. Chen Z, Zhang C, Zhou T, Ma H (2015) Gold nanoparticle based colorimetric probe for dopamine detection based on the interaction between dopamine and melamine. Microchim Acta 182:1003–1008. https://doi.org/10.1007/s00604-014-1417-0
34. Li Y, Lin H, Peng H, Qi R, Luo C (2016) A glassy carbon electrode modified with MoS2 nanosheets and poly(3,4-ethylenedioxythiophene) for simultaneous electrochemical detection of ascorbic acid, dopamine, and uric acid. Microchim Acta 183:2517–2523. https://doi.org/10.1007/s00604-016-1897-1
35. Kavitha T, Yuvaraj H (2011) Facile approach to the synthesis of high-quality NiO nanorods: electrochemical and antibacterial properties. J Mater Chem 21(39):15686–15691. https://doi.org/10.1039/ C1JM13278D